

Investigations of High Rate Capability and High Temperature Performance for Nano-Sized Porous $\text{LiAl}_x\text{Mn}_{2-x}\text{O}_4$ ($x=0, 0.05, 0.1, 0.15$) Cathode Material

Huayun Xu, Bin Cheng, Endai Xu, Liqiang Xu, Jian Yang*, Yitai Qian

Key Laboratory of the Colloid and Interface Chemistry (Shandong University), Ministry of Education, and School of Chemistry and Chemical Engineering, Shandong University, Jinan 250100, PR China

*E-mail: xuhuayun@sdu.edu.cn

Received: 26 September 2012 / Accepted: 15 October 2012 / Published: 1 December 2012

Porous $\text{LiAl}_x\text{Mn}_{2-x}\text{O}_4$ ($x=0, 0.05, 0.1, 0.15$) nanoparticles were synthesized by sol-gel method. Differential scanning calorimetry and thermogravimetric analysis (DSC/TGA) were applied to determine the phase transition temperature and the decomposition temperature of precursors. X-ray diffraction (XRD) was used to characterize the phase composition. Cyclic voltammetry (CV), electrochemical impedance spectroscopy (EIS) and direct current resistance (DC) were carried out to analyze the thermodynamic and kinetic behaviors during lithium insertion and removal for $\text{Li}/\text{LiAl}_x\text{Mn}_{2-x}\text{O}_4$ ($x=0, 0.05, 0.1, 0.15$) electrodes. After Al doped, charge transfer resistance decreases and DC resistance increasing at the end of discharge is impressed. When charged at 5 C rate, $\text{Li}/\text{LiAl}_{0.1}\text{Mn}_{1.9}\text{O}_4$ electrode shows the reversible capacities of 96 mAh g^{-1} at 50 C discharge rate, and the power and energy densities is 26.6 kW kg^{-1} and 359 Wh kg^{-1} , respectively. At $55 \text{ }^\circ\text{C}$, $\text{LiAl}_{0.1}\text{Mn}_{1.9}\text{O}_4$ sample performs reversible capacity of 112.1 mAh g^{-1} and 85% initial capacity is retained after 200 cycles at 5 C charge/discharge rate. Improved reversibility and decreased charge transfer resistance is found for $\text{LiAl}_{0.1}\text{Mn}_{1.9}\text{O}_4$ sample with elevated temperature by CV and EIS analysis.

Keywords: Spinel; Al doped spinel; High rate capability; Cyclic voltammetry; Electrochemical impedance spectroscopy; Direct current resistance

1. INTRODUCTION

In recent years, high power lithium-ion batteries are increasingly required due to high power applications in hybrid electric vehicles, portable power tools and medical equipments [1–3]. Cathode materials are the key component of lithium-ion batteries that directly determines the power density. Lithium manganese oxide, LiMn_2O_4 , with the cubic spinel structure, is one of promising alternative cathode materials for lithium-ion batteries by virtue of high potential, low cost, low toxicity and good

safety [4, 5]. However, how to improve the energy and power density and cyclic stability especially at a high temperature such as 55°C for LiMn_2O_4 is still a challenge for both scientists and engineers [6]. Various methods have been developed to increase the power density for cathode materials, such as nanocrystallizing [7-9], coating [10-12] or doping [6, 13]. And it has well been demonstrated that the electrochemical performance of LiMn_2O_4 could be improved by partial substitution of Mn^{3+} with several elements, such as Co [14,15], Cr [16], Zn [17], Ce [18], Li [19] Al [20-26], Fe [27,28], Ni [29,30] and Mg [31] etc. The mechanism of doping mainly lies in several aspects such as increasing lattice constant to promote lithium ion diffusion in host electrode materials [16], elevating the average valence of Mn ion to impress Jahn-Teller effect [17], increasing the electrical conductivity to improve specific capacity [29] and enhancing the spinel structure to decrease Mn ion dissolving in organic electrolyte [30] and so on.

Compared to Co, Cr, V and Ni etc, Aluminum is nontoxic, inexpensive and abundant. Moreover, stronger bond energy of Al–O ($\sim 501.9 \text{ kJ mol}^{-1}$) compared to Mn–O ($\sim 362 \text{ kJ mol}^{-1}$) in spinel oxide could stabilize the structure of LiMn_2O_4 especially at high temperature during charge/discharge course and associated material dissolution [32-34]. In recent decade, some papers reported the electrochemical property of Al doped LiMn_2O_4 [20-26]. Lee reported $\text{LiAl}_x\text{Mn}_{2-x}\text{O}_4$ for the lithium secondary battery in 2001. It was obtained initial capacity of 128 mAh g^{-1} and 115 mAh g^{-1} after 100 cycles with a discharge current of 0.4 mA cm^{-2} [20]. Hwang investigated Al-doped LiMn_2O_4 spinel synthesized by a sol-gel method, which showed the initial and 10th discharge capacity were about of 100 mAh g^{-1} and 90 mAh g^{-1} respectively at 0.1C charge/discharge rate [21]. Yi synthesized $\text{LiAl}_x\text{Mn}_{2-x}\text{O}_4$ samples and found that $\text{LiAl}_{0.05}\text{Mn}_{1.95}\text{O}_4$ performed the best electrochemical property with 123.9 mAh g^{-1} at 0.15 C charge/discharge rate and maintained 94.2 mAh g^{-1} after 50 cycles [22]. Thirunakaran reported that $\text{LiAl}_{0.1}\text{Mn}_{1.9}\text{O}_4$ spinel was found to deliver discharge capacity of 139 mAh g^{-1} at C/10 rate during the first cycle and maintained 97 mAh g^{-1} after 10cycles [25]. Al doped LiMn_2O_4 samples prepared by the wet-milling method, achieved up to 99% of retention of capacity charged at 50 mA g^{-1} at $50 \text{ }^\circ\text{C}$ after 30th cycle reported by Kakuda [26]. However, fast charge and discharge performances especially at an elevated temperature were lack for most published Al doping LiMn_2O_4 literatures. Thermodynamic and kinetic behaviors at a high temperature such as $55 \text{ }^\circ\text{C}$ were seldom studied.

In our previous work, we reported $\text{LiM}_{0.1}\text{Mn}_{1.9}\text{O}_4$ (M=Mn, Al, Fe) material, $\text{Li/LiAl}_{0.1}\text{Mn}_{1.9}\text{O}_4$ cell shows better rate capability than pristine and Fe doping spinel [35]. In this work, $\text{LiAl}_x\text{Mn}_{2-x}\text{O}_4$ ($x=0, 0.05, 0.1, 0.15$) nanoparticles were synthesized by a sol-gel method. Charge–transfer resistance (R_{ct}) and in-site DC resistance for $\text{LiAl}_x\text{Mn}_{2-x}\text{O}_4$ ($x=0, 0.05, 0.1, 0.15$) were investigated by EIS and DC resistance tests. The thermodynamic and kinetic behaviors during lithium insertion and removal for $\text{LiAl}_{0.1}\text{Mn}_{1.9}\text{O}_4$ sample at elevated temperature were also studied.

2. EXPERIMENTAL

2.1. Preparation of materials

The $\text{LiAl}_x\text{Mn}_{2-x}\text{O}_4$ ($x=0, 0.05, 0.1, 0.15$) were prepared by sol-gel method using citric acid and glycol as the chelating agents. The stoichiometric amount of lithium nitrate LiNO_3 (CP), 50wt %

manganese nitrate $\text{Mn}(\text{NO}_3)_2$ solution (AR), aluminum nitrate $\text{Al}(\text{NO}_3)_3 \cdot 9\text{H}_2\text{O}$ (AR) were mixed with citric acid (AR) and glycol (AR) which their molar ratio was kept as 1:4 dissolved in 20 mL of distilled water. The molar ratio of metal ion to citric acid was kept at 1:1. Then the solution was stirred at 80 °C for 2 h, and the obtained gel was dried in air at 180°C for 10 h. After that, the product was slowly heated to 700 °C at a rate of 5 °C min^{-1} and was kept at that temperature for 10 h. Finally, the product was cooled to room temperature for the later use.

2.2. Characterization of $\text{LiAl}_x\text{Mn}_{2-x}\text{O}_4$ ($x=0, 0.05, 0.1, 0.15$) compounds

The XRD patterns of the product were recorded on a Bruker D8 advanced X-ray diffractometer equipped with Ni-filtered Cu $K\alpha$ radiation ($\lambda=1.5418\text{\AA}$).

2.3. Preparation and electrochemical testing of composite electrodes

The composite electrodes were prepared as follow: active material, acetylene black and PVDF binder in the mass ratio of 8: 1: 1 were mixed in N-methyl-2-pyrrolidone to form slurry. The slurry was coated onto an Al-foil current collector, and dried at 80 °C for 12h. The coin cells of type CR2032 were made in an Ar-filled glove box using lithium metal foil as the counter and the reference electrode. The electrolyte used was LiPF_6 in ethylene carbonate, diethyl carbonate, dimethyl carbonate in the ratio of 1:1:1 by volume. The galvanostatic studies were carried out with a LAND CT2001A auto-cycler (China) in the voltage range of 3.4~4.3V at 25 °C and at 55 °C. CV experiments were conducted between 3.4~4.3 V at a scan rate from 0.1 to 1 mV s^{-1} using a LK2005A Electrochemical Workstation. EIS for fresh assembled electrodes were performed by a Zahner Elektrik IM6 (Germany) impedance instrument over the frequency range of 100 kHz to 0.01 Hz. The internal resistance of the cells was also measured by a current interruption technique and the method was ever introduced by Chen [36].

3. RESULTS AND DISCUSSION

Figure 1 shows the DSC-TGA curves for the precursor of LiMn_2O_4 prepared by sol-gel method. The weight loss between the room temperature and 210 °C is attributed to the removal of water and glycol adsorbed on the surface. From 210 °C to 350 °C, there is a huge weight loss in the TGA curve. Corresponding to this weight loss, the DSC curve presents three exothermic peaks, which is probably due to the pyrolysis of the organic components and the formation of spinel phase. This result also indicates that the annealing temperature of the precursor must be higher than 350 °C to ensure the complete decomposition of organic components and the formation of LiMn_2O_4 . After that, there is no obvious weight loss from 350 °C to 800 °C, reflecting the good thermal stability of the product.

Figure 2a shows XRD patterns of $\text{LiAl}_x\text{Mn}_{2-x}\text{O}_4$ ($x=0, 0.05, 0.1, 0.15$) samples. The diffraction peaks of the samples are identified as the spinel phase in the cubic $Fd-3m$ space group (JCPDS Card,

No.35-782). The lattice parameters calculated from these XRD patterns (Figure. 2b) monotonously decreases from 8.228(0) to 8.209(1) Å with the increasing Al from 0 to 0.15, which could be assigned to the smaller radius of Al³⁺ (0.053 nm) than those of Mn³⁺ (0.066 nm) and Mn⁴⁺ (0.060 nm) [37], and the stronger bond energy of Al-O (501.9±10.6 kJ mol⁻¹) than Mn-O (362±25 kJ mol⁻¹) [33]. It is believed that Al atoms have successfully occupied the sites of manganese in our pristine samples.

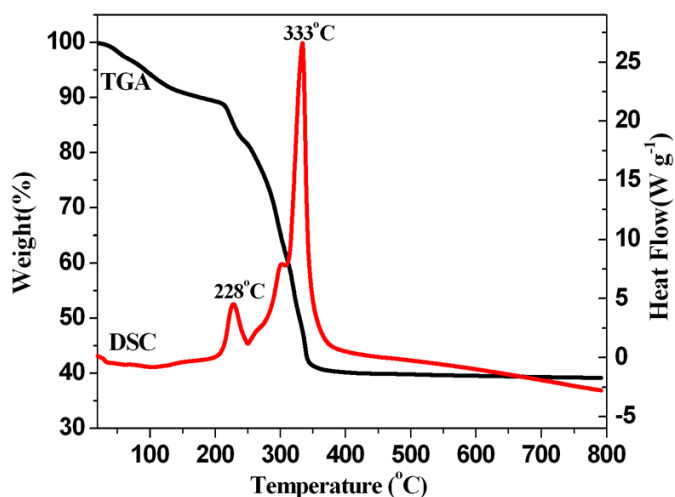


Figure 1. DSC-TGA curves for the precursor of LiMn₂O₄

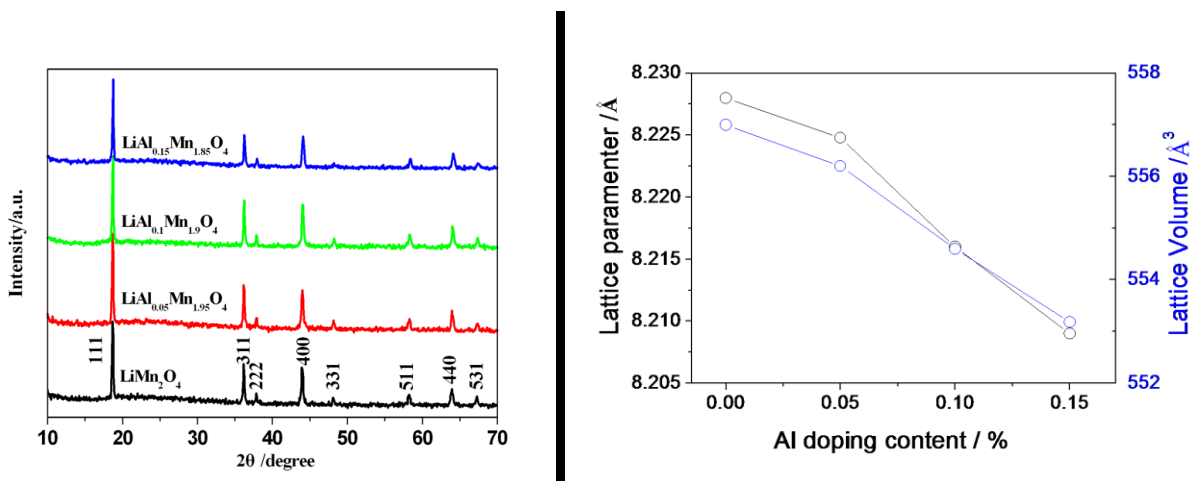


Figure 2. XRD patterns of LiAl_xMn_{2-x}O₄ (x=0, 0.05, 0.1, 0.15) powders (a); Lattice parameters and volume values for LiAl_xMn_{2-x}O₄ powders (b)

The surface morphology and particle size distribution are the important factors to affect the electrochemical property of the lithium ion batteries, so particle size and morphology of the powders without and with Al doping have been examined by SEM and TEM as shown in Figure 3a-3d in reference [35]. Both LiMn₂O₄ and LiAl_{0.1}Mn_{1.9}O₄ show porous morphology, composed of interconnected nano-sized particles (60~90 nm). The porous morphology may be attributed to citric

acid and glycol that form a complex organic network where the metal ions are uniformly distributed in the matrix, and the resultant gel is of atomic scale and homogeneously mixed with each other. Thus, during thermal decomposition process it may be able to prevent phase separation and lead to the formation of homogeneous nano-sized particles. The porous structure with a narrow size distribution and relatively large surface is expected to benefit discharge capacity and rate capability for Li-Al-Mn-O spinel cathode materials.

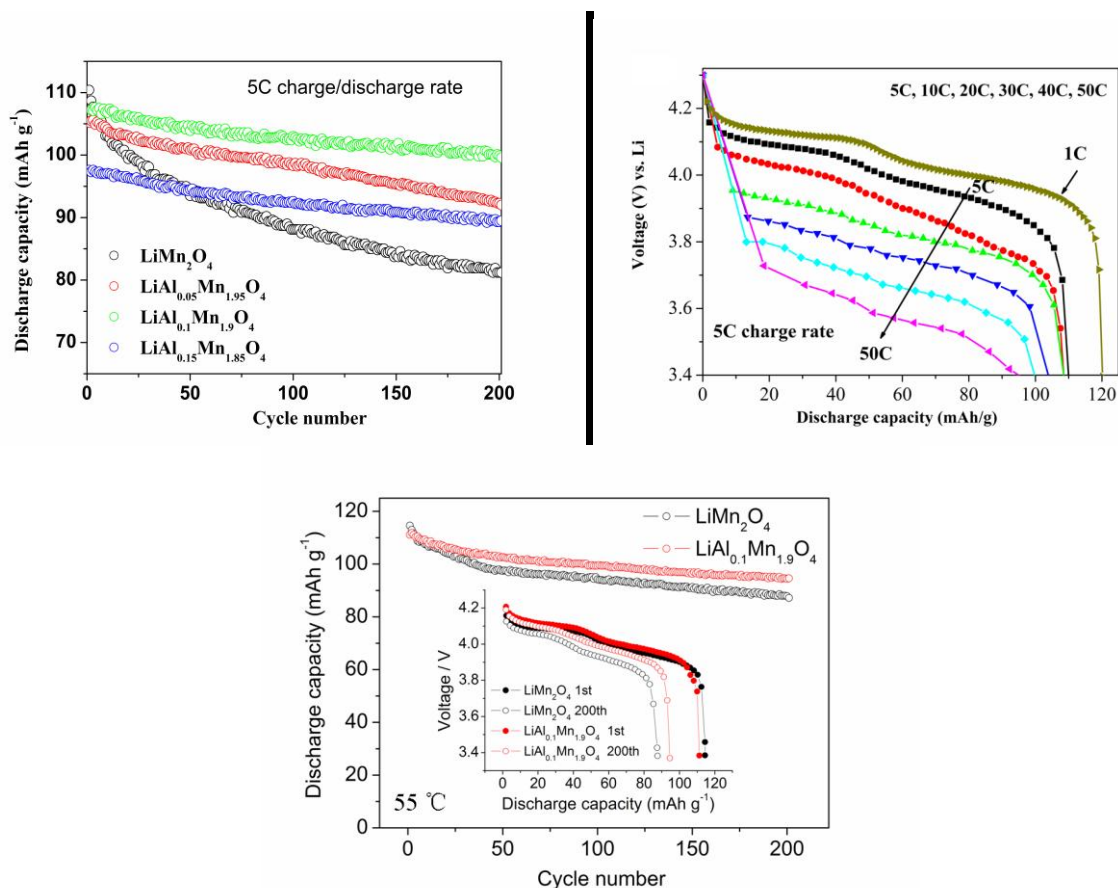


Figure 3. The cycle performance of Li/LiAl_xMn_{2-x}O₄ (x=0, 0.05, 0.1, 0.15) electrodes at 5 C charge and discharge rate (a); Discharge profile for Li/LiAl_{0.1}Mn_{1.9}O₄ electrodes at varied discharged rate (b); Cyclability and charge/discharge profile of Li/LiMn₂O₄ and Li/LiAl_{0.1}Mn_{1.9}O₄ electrodes at 5C charge and discharge rate at 55 °C(c)

The cycle performance of LiAl_xMn_{2-x}O₄ (x=0, 0.05, 0.1, 0.15) samples at 5 C charge and discharge rate is presented in Figure 3a. The initial charge/discharge capacity for LiAl_xMn_{2-x}O₄ samples reduces from 112 to 98 mAh g⁻¹, as x increases from 0 to 0.15. This suggests that only the amount of Mn contributes the charge/discharge capacity during the electrochemical reaction. Although the initial capacity is lower than that of pristine LiMn₂O₄, long-term cycling performance is significantly improved with the increase of Al dopant. After 200 cycles at 5 C charge/discharge rate, over 108.2 mAh g⁻¹ with 94% capacity retention for LiAl_xMn_{2-x}O₄ when x=0.1 is obtained, much better than 80 mAh g⁻¹ of LiMn₂O₄ with a capacity retention of 73% . It is thought that the stronger bond

energy of Al–O ($\sim 501.9 \text{ kJ mol}^{-1}$) than Mn–O ($\sim 362 \text{ kJ mol}^{-1}$) is contributed to avoid the Jahn-Teller distortion and then stabilizes spinel structure during lithium insertion and removal reaction [34]. Nevertheless, the $\text{LiAl}_{0.1}\text{Mn}_{1.9}\text{O}_4$ sample shows the best electrochemical performance among the synthesized $\text{LiAl}_x\text{Mn}_{2-x}\text{O}_4$ ($x=0, 0.05, 0.1, 0.15$) samples.

To investigate the application for high power density devices, $\text{Li}/\text{LiAl}_{0.1}\text{Mn}_{1.9}\text{O}_4$ electrode were discharged from 5 C to 50 C rate (charged at 5 C rate) as presented in Figure 3b. It is noticed that the two discharge plateaus for $\text{Li}/\text{LiAl}_{0.1}\text{Mn}_{1.9}\text{O}_4$ electrode evolve to one with increasing discharge rate resulting from increased polarization resistance. On the other hand, the $\text{Li}/\text{LiAl}_{0.1}\text{Mn}_{1.9}\text{O}_4$ electrode exhibits relatively high specific capacity at high discharge rate (5 C: 111.6 mAh g^{-1} , 10 C: 110.5 mAh g^{-1} , 20 C: 110.7 mAh g^{-1} , 30 C: 109.8 mAh g^{-1} , 40 C: 101.6 mAh g^{-1} , 50 C: 96 mAh g^{-1} , respectively) compared to published data [17-20, 22, 23, 27, 38, 39].

Table 1. Electrochemical performance comparison of published data for Al or other doping positive ion for LiMn_2O_4 and results in our work at 25 °C and 55 °C

Sample	Rate capability parameters		Initial capacity (mAh/g)	Cycles number	Capacity retention (%)	T(° C)	Reference
	Charge rate	Discharge rate					
$\text{LiAl}_{0.15}\text{Mn}_{1.85}\text{O}_4$	0.1C	0.1C	100	10	90	RT	[27]
$\text{LiAl}_{0.1}\text{Mn}_{1.9}\text{O}_4$	0.15C	0.15C	117.9	50	95	RT	[22]
$\text{LiAl}_{0.09}\text{Mn}_{1.91}\text{O}_4$	0.4 mA cm^{-2}	0.4 mA cm^{-2}	128.7	100	90	RT	[20]
$\text{LiAl}_{0.05}\text{Mn}_{1.9}\text{O}_4$	1/3C	1C	107.7	50	86.6	RT	[23]
$\text{LiCe}_{0.05}\text{Mn}_{1.95}\text{O}_4$	0.5C	15C	102	100	87	RT	[18]
$\text{LiZn}_{0.10}\text{Mn}_{1.90}\text{O}_4$	0.5C	15C	92	100	77.2	RT	[17]
$\text{LiCo}_{1/6}\text{Mn}_{11/6}\text{O}_4$	5C	5C	86	200	99	RT	[38]
$\text{LiAl}_{0.1}\text{Mn}_{1.9}\text{O}_4$	5C	5C	108.2	500	92.4	25	This work
LiMn_2O_4	1C	50C	70	—	—	RT	[39]
LiMn_2O_4	5C	50C	79	—	—	RT	This work
$\text{LiMn}_{1.93}\text{Li}_{0.06}\text{Al}_{0.01}\text{O}_4$	0.5C	1C	105.7	100	90.3	55	[19]
$\text{LiCe}_{0.05}\text{Mn}_{1.95}\text{O}_4$	0.5C	5C	69	100	66.7	60	[18]
$\text{LiAl}_{0.1}\text{Mn}_{1.9}\text{O}_4$	5C	5C	112.1	200	85.0	55	This work

To evaluate the cycling stability at elevated temperature, we studied the electrochemical performance of LiMn_2O_4 and $\text{LiAl}_{0.1}\text{Mn}_{1.9}\text{O}_4$ at 5C charge/discharge rate at 55°C as given in Figure 3c. $\text{LiAl}_{0.1}\text{Mn}_{1.9}\text{O}_4$ sample performs reversible capacity of 112.1 mAh g^{-1} and 85% initial capacity is retained after 200 cycles while 114.8 mAh g^{-1} and capacity retention of only 69 % is found for LiMn_2O_4 sample. It should be attributed to better structural stability against oxygen loss and less distinctive structural changes during cycling at high temperature (55°C) for Al-doped sample according to Chung' results [33]. Table 1 summarizes the published data for aluminum or other doping positive ion for LiMn_2O_4 and our results at 25°C and 55°C .

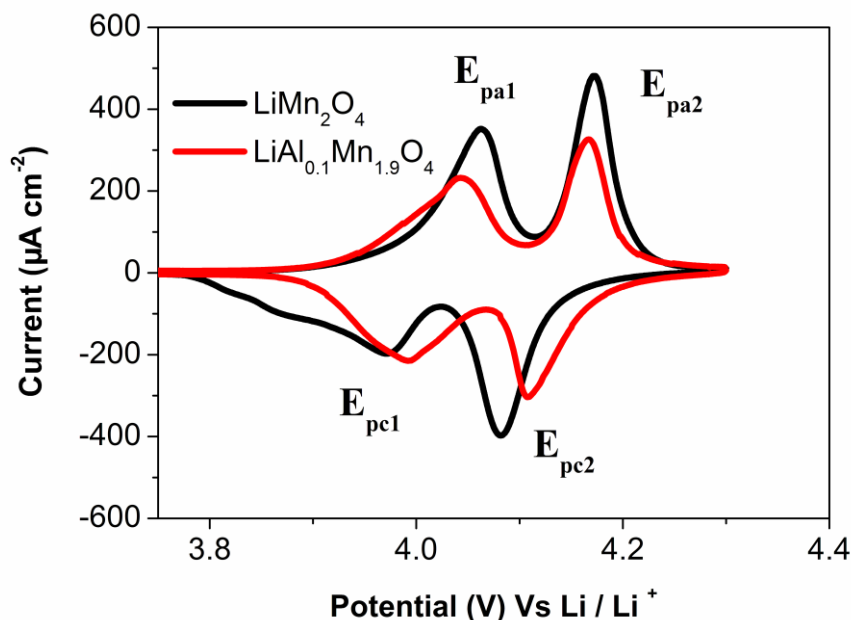


Figure 4. Cyclic voltammograms (CVs) of $\text{Li}/\text{LiMn}_2\text{O}_4$ electrode and $\text{Li}/\text{LiAl}_{0.1}\text{Mn}_{1.9}\text{O}_4$ electrode at the sweeping rate of 0.1 mV s^{-1}

The CVs of the LiMn_2O_4 and $\text{LiAl}_{0.1}\text{Mn}_{1.9}\text{O}_4$ electrodes tested at the same rate of 0.1 mV s^{-1} are compared as shown in Figure 4. The cathodic peaks shift to high potential for $\text{LiAl}_{0.1}\text{Mn}_{1.9}\text{O}_4$ compared to pristine LiMn_2O_4 sample. This observation coincides with the galvanostatic results that the $\text{LiAl}_{0.1}\text{Mn}_{1.9}\text{O}_4$ electrodes exhibit higher discharge plateaus, which indicates improved plateau efficiency compared to LiMn_2O_4 sample. The separation of peak potentials of the cathodic and anodic peaks for $\text{LiAl}_{0.1}\text{Mn}_{1.9}\text{O}_4$ are 50 mV and 60 mV, obviously lower than those of pure LiMn_2O_4 sample (100 mV and 110 mV) indicating that lithium inserting reaction of $\text{LiAl}_{0.1}\text{Mn}_{1.9}\text{O}_4$ is in a more equilibrium state, behaving more likely as a Nernst system. This result is consistent with the electrochemical property for $\text{LiAl}_{0.1}\text{Mn}_{1.9}\text{O}_4$ which behaves improved discharge plateau efficiency and reversibility compared to LiMn_2O_4 spinel as discussed above.

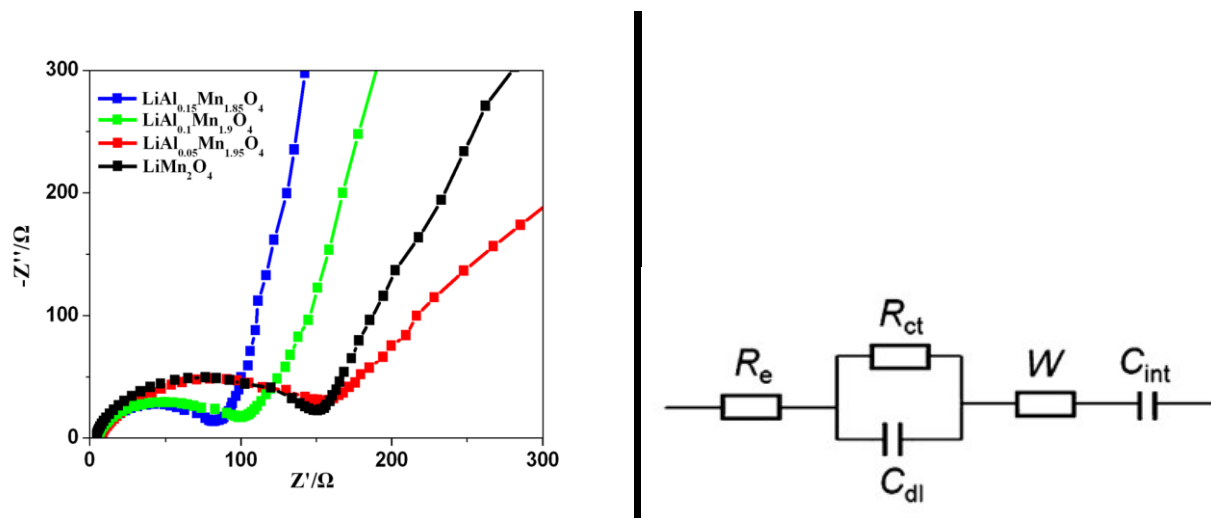


Figure 5. Nyquist plots for Li/LiAl_xMn_{2-x}O₄ (x=0, 0.05, 0.1, 0.15) electrodes (a) and fitting equivalent circuit (b)

Figure 5a shows the EIS of Li/LiAl_xMn_{2-x}O₄ (x=0, 0.05, 0.1, 0.15) electrodes composed of a semicircle and a straight sloping line. The equivalent circuit for modeling impedance data is shown in Figure 5b. The intercept at the real (Z') axis in high frequency corresponds to the ohmic electrolyte resistance (R_e). The semicircle in the middle frequency range indicates the charge transfer resistance (R_{ct}) and C_{dl} is its relative double layer capacitance. The inclined straight line relates to the Warburg impedance (Z_w) which is combined with the diffusional effects of Li^+ . C_{int} is the reflection of intercalation capacitance [40]. It can be seen that the R_e values of different samples are almost constant, whereas R_{ct} values vary greatly with the Al doping and decreases from 152.4 Ω to 79.3 Ω with x changing from 0 to 0.15 as shown in Figure 5a. The minimum R_{ct} value of LiAl_{0.15}Mn_{1.85}O₄ which is far lower than that of the undoped sample means a lower electrochemical polarization, and this leads to improved fast charge/discharge capability. The Z_w values of LiMn₂O₄ and LiAl_{0.1}Mn_{1.9}O₄ obtained by fitting the impedance data are 57.4 Ω and 65.7 Ω , respectively.

DC resistance of LiMn₂O₄ and LiAl_{0.1}Mn_{1.9}O₄ samples as a function of depth of discharge (DOD) was performed to investigate the in-site resistance change during the whole discharge course as given in Figure 6. In the beginning stage of the charge step, cell resistance for both electrodes decreases quite rapidly and reaches a minimum at the DOD of 20~25%. Then the resistance increases to a relatively high value and drops again to another minimum value at DOD of 50~55%, and undergoes rapid increase for the rest of depth of discharge especially for pristine LiMn₂O₄ sample. Clearly, each curve has two minimum resistance values forming a “w”-shape curve part, which is ever found for LiNi_{0.5}Mn_{1.5}O₄ cathode material by Chen’ group [36] and the appearance of the “w” shape curve corresponds to a two-plateau characteristic for LiMn₂O₄ and LiAl_{0.1}Mn_{1.9}O₄ electrodes, which is consistent with the CV peak position (Figure 4).

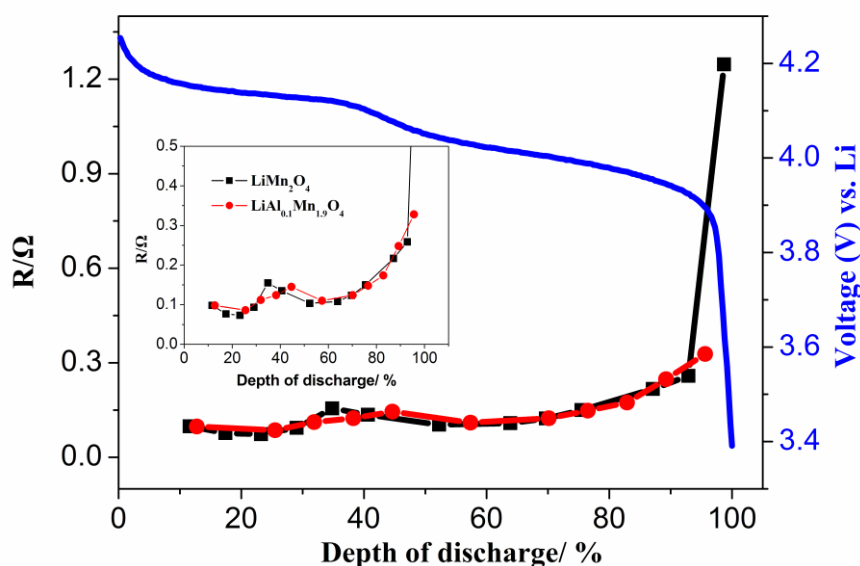


Figure 6. DC resistance of Li/LiMn₂O₄ and Li/LiAl_{0.1}Mn_{1.9}O₄ electrodes as function of depth of discharge (DOD)

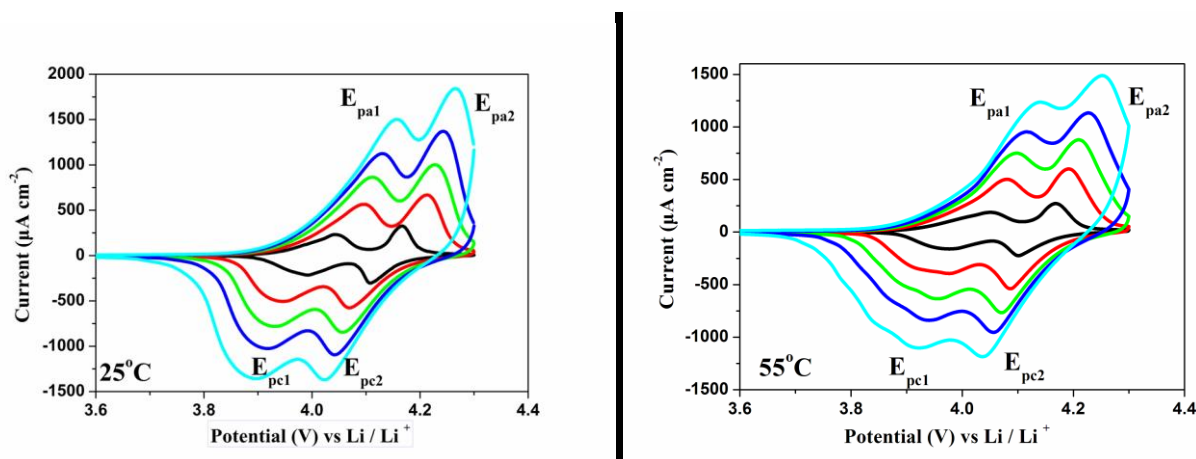


Figure 7. CVs of Li/LiAl_{0.1}Mn_{1.9}O₄ electrode recorded at different potential sweeping rates 0.1, 0.2, 0.3, 0.5, 0.7 and 1 mV s⁻¹ at 25 °C (a) and 55 °C (b); CVs Li/LiAl_{0.1}Mn_{1.9}O₄ electrodes tested at the same rate of 0.5 mV s⁻¹ at 25 °C and 55 °C (c)

It is also found an obvious decade of increase in DC resistance profile after the doping of Al in spinel LiMn₂O₄. Nevertheless, the resistance before 95 % depth of discharge for both samples is similar. However, a rapidly increasing resistance occurs after 95 % DOD for LiMn₂O₄ sample compared to Al doping spinel. It is suggested that at the end of discharge, structure transformation from cubic to tetragonal phase occurs and is impressed by Al doping owing to stronger bond energy of Al–O than Mn–O and the increased average valence of Mn ion compared to pristine spinel LiMn₂O₄.

Figure 7a and 7b show the CVs of the $\text{LiAl}_{0.1}\text{Mn}_{1.9}\text{O}_4$ recorded at different potential sweeping rates from 0.1 to 1 mV s^{-1} at 25 °C and 55 °C. The electrodes tested at two temperature show increasing peaks current density (I_p) and widening separation potential within each redox couple as the potential scanning rate (v) increases. The separation of peak potentials of the cathodic and anodic peaks for $\text{LiAl}_{0.1}\text{Mn}_{1.9}\text{O}_4$ at 25 °C are 50 mV and 60 mV, similar to that at 55 °C sample (70 mV and 70 mV) at the sweeping rate of 0.1 mV s^{-1} . However, the separation values of peak potentials changed from 260 mV and 250 mV for samples at 25°C to 220 mV and 210 mV for samples at 55 °C when increasing the sweeping rate to 1 mV s^{-1} . The separation of peak potentials at varied scanning rates for $\text{LiAl}_{0.1}\text{Mn}_{1.9}\text{O}_4$ at 25 °C and 55 °C were summarized in Table 2.

Table 2. The separation of peak potentials at varied scanning rates for $\text{LiAl}_{0.1}\text{Mn}_{1.9}\text{O}_4$ samples at 25 °C and 55 °C

$\text{LiAl}_{0.1}\text{Mn}_{1.9}\text{O}_4$		0.1 mVs^{-1}	0.3 mVs^{-1}	0.5 mVs^{-1}	0.7 mVs^{-1}	1 mVs^{-1}
ΔE_1	25 °C	50	105	180	220	260
	55 °C	70	110	150	170	220
ΔE_2	25 °C	60	140	160	200	250
	55 °C	70	110	140	170	210

CVs of the two spinel electrodes tested at the same rate of 0.5 mV s^{-1} were given in Figure 7c. The $\text{LiAl}_{0.1}\text{Mn}_{1.9}\text{O}_4$ electrode displays less redox couple separation (ΔE_{p1}) between E_{pa1} and E_{pc1} at 55 °C than that at 25 °C. Therefore, it is suggested that lithium inserting reaction of $\text{LiAl}_{0.1}\text{Mn}_{1.9}\text{O}_4$ at 55 °C is closer to the thermodynamic equilibrium state than that at 25 °C, which are reflected in their cycling performance as shown in Figure 3a and 3c.

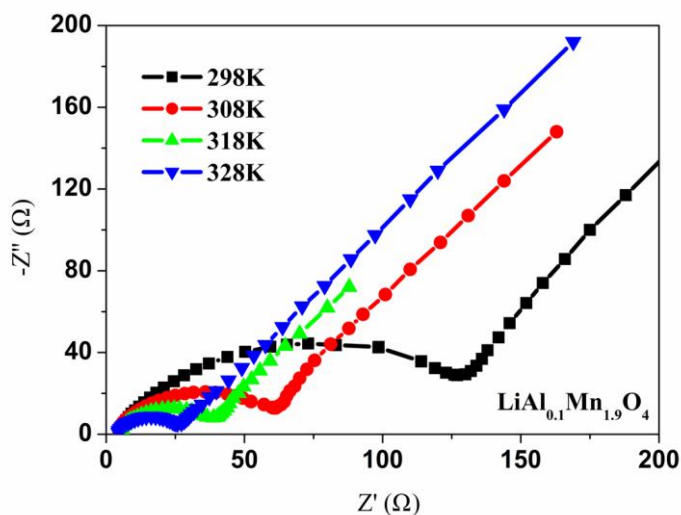


Figure 8. Nyquist plots of the $\text{Li}/\text{LiAl}_{0.1}\text{Mn}_{1.9}\text{O}_4$ electrodes tested at different temperatures

Figure 8 shows the Nyquist plots of the fresh assembled Li/LiAl_{0.1}Mn_{1.9}O₄ electrodes at different temperatures. As the temperature increases, charge-transfer resistance R_{ct} gradually decreases from 125 Ω to 25 Ω . Clearly, elevated temperature fastens charge transfer kinetics. Though R_{ct} is impressed, cyclic stability of the Li/LiAl_{0.1}Mn_{1.9}O₄ electrode at 55 °C (Figure 3c) deteriorates compared to that at 25°C (Figure 3a). The formation of degradation products (Li₂MnO₃, γ -MnO₂) and new phase formation in LiAl_{0.1}Mn_{1.9}O₄ could contribute to the capacity fading due to active material loss and more importantly by affecting the kinetics of Li ion in the electrode [41]. Meanwhile, the lithium ion diffusion coefficient could be calculated using the following equation [42]:

$$D = 0.5 (RT/AF^2C\sigma)^2 \quad (1)$$

Herein, R is the gas constant, T is the absolute temperature, A is the surface area of the electrode, F is the Faraday constant, C is the concentration of lithium ions, and s is the Warburg impedance coefficient which is associated with Z_{re} .

$$Z_{re} = R_e + R_{ct} + \sigma\omega^{-1/2} \quad (2)$$

Herein, R_e is the electrolyte resistance, R_{ct} is the charge transfer resistance, ω is the angular frequency in the low frequency. The parameters of the equivalent circuit and diffusion coefficients of the LiAl_{0.1}Mn_{1.9}O₄ are calculated and are in the range of $1 \times 10^{-9} \sim 10^{-10} \text{ cm}^2 \text{ s}^{-1}$. There is no obvious change for D_{Li+} in the *temperature* range between 25 °C and 55 °C. Our D_{Li+} values are in good agreement with the reported result about Li (M_{1/6}Mn_{11/6}) O₄ (M=Mn, Co, CoAl) materials at ambient temperature and 50 °C [41].

4. CONCLUSIONS

LiAl_xMn_{2-x}O₄ (x=0, 0.05, 0.1, 0.15) were synthesized via sol-gel route. XRD shows that all the samples exhibit pure spinel phase. CV, EIS and in site DC tests reveals that R_{ct} decreases and DC resistance increasing at the end of discharge is impressed after Al doping. More reversibility and fast charge transfer for the lithium insertion/removal reaction in LiAl_{0.1}Mn_{1.9}O₄ is observed with elevated temperature by CV and EIS tests. D_{Li+} for LiAl_{0.1}Mn_{1.9}O₄ sample in the *temperature* range between 25 °C and 55 °C are in the range of $1 \times 10^{-9} \sim 10^{-10} \text{ cm}^2 \text{ s}^{-1}$. The LiAl_{0.1}Mn_{1.9}O₄ synthesized in our work is a promising cathode material for applications in both EVs and HEVs.

ACKNOWLEDGEMENTS

This study was supported by the 973 Project of China (No.2011CB935901), the National Natural Science Foundation of China (Grant No. 21203111, 11179043, 91022033), the Independent Innovation Foundations of Shandong University (2011GN032, 2012ZD007), Shandong Provincial Natural Science Foundation for Distinguished Young Scholar and start-up funding for new faculties in Shandong University.

References

1. A.Y. Shenouda, H.K. Liu, *J. Alloy Compd.* 477 (2009) 498-503.
2. J. Tu, X.B. Zhao, J. Xie, G.S. Cao, D.G. Zhuang, *J. Alloy Compd.* 432 (2007) 313-317.
3. K. Tatsumi, *J Asian Electric Vehicles* 8 (2010) 1415-1418.
4. M.M. Thackeray, *J. Electrochem. Soc.* 142 (1995) 2558-2563.
5. H. Sahan, H. Goktepe, S. Patat, *J. Alloy Compd.* 509 (2011) 4235-4241.
6. A.B. Yuan, L. Tian, W.M. Xu, Y.Q. Wang, *J. Power Sources* 195 (2010) 5032-5038.
7. H.W. Lee, P. Muralidharan, R. Ruffo, C.M. Mari, Y. Cui, D.K. Kim, *Nano Lett.* 10 (2010) 3852-3856.
8. K. Du, H. Zhang, *J. Alloy Compd.* 352 (2003) 250-254.
9. V. Koleva, E. Zhecheva, R. Stoyanova, *J. Alloy Compd.* 476 (2009) 950-957.
10. K.H. Jung, H.G. kim, Y.J. Park, *J. Alloy Compd.* 509 (2011) 4426-4432.
11. H.B. Kim, B.C. Park, S.T. Myung, K. Amine, J. Prakash, Y.K. Sun. *J. Power Sources* 179 (2008) 347-350.
12. X.W. Li, R. Yang, B. Cheng, *Mater. Lett.* 66 (2012) 168-171.
13. M. Akhalouch, J.M. Amarilla, R.M. Rojas, I. Saadoun and J.M. Rojo, *Electrochem. Commun.* 12 (2010) 548-552.
14. F.A. Amaral, N. Bocchi, R.F. Brocenschi, S.R. Biaggio and R.C. Rocha-Filho, *J. Power Sources* 195 (2010) 3293-3301.
15. X.J. Sun, X.H. Hu, Y. Shi, S.X. Li and Y.Q. Zhou, *Solid State Ionics* 180 (2009) 377-384.
16. W.M. Xu, A.B. Yuan, L. Tian and Y.Q. Wang, *J Appl. Electrochem.* 41 (2011) 453-460.
17. D. Arumugam, G.P. Kalaignan, K. VEDIAPPAN and C.W. Lee, *Electrochim. Acta* 55 (2010) 8439-8444.
18. D. Arumugam and G.P. Kalaignan, *J. Electroanal. Chem.* 648 (2010) 54-59.
19. J.M. Amarilla, K. Petrov, F. Picó, G. Avdeev, J. M. Rojo and R. M. Rojas, *J. Power Sources* 191 (2009) 591-600.
20. Y.S. Lee, N. Kumada and M. Yoshio, *J. Power Sources* 96 (2001) 376-384.
21. B.J. Hwang, R. Santhanam, D.G. Liu and Y.W. Tsai, *J. Power Sources* 102 (2001) 326-331.
22. T.F. Yi, Y. R. Zhu, R. S. Zhu, L. Zhou, P. Li and J. Shu, *Ionics* 15 (2009) 177-182.
23. T.F. Yi, X. G. Hu and K. Gao, *J. Power Sources* 162 (2006) 636-643.
24. S.J. Bao, Y.Y. Liang, W.J. Zhou, B.L. He and H. L. Li, *J. Power Sources* 154 (2006) 239-245.
25. R. Thirunakaran, A. Sivashanmugam, S. Gopukumar, C.W. Dunnill, D.H. Gregory, *J. Phys. Chem. Solids* 69 (2008) 2082-2090.
26. T. Kakuda, K. Uematsu, K. Toda, M. Sato, *J. Power Sources* 167 (2007) 499-503.
27. H.J. Bang, V.S. Donepudi, J. Prakash, *Electrochim. Acta* 48 (2002) 443-451.
28. Q. Luo and A. Manthiram, *J. Electrochem. Soc.* 156 (2009) A84-A88.
29. Y. Tomita, H. Yonekura, K. Kobayashi. *Bull. Chem. Soc. Jpn.* 77 (2002) 2253-2256.
30. S. Ivanova, E. Zhecheva, R. Stoyanova, D. Nihtianova, S. Wegner, P. Tzvetkova, S. Simova. *J. Phys. Chem. C* 115 (2011) 25170-25182.
31. X. Gu, X.W. Li, L.Q. Xu, *Int. J. Electrochem. Sci.* 7 (2012) 2504-2512.
32. L. F. Xiao, Y.Q. Zhao, Y. Y. Yang, Y. L. Cao, X. P. Ai, *Electrochim. Acta* 54 (2008) 545-550.
33. K.Y. Chung, W.S. Yoon, H.S. Lee, X.Q. Yang, *J. Power Sources* 146 (2005) 226-231.
34. S.T. Myung, S. Komaba, N. Kumagai, *J. Electrochem. Soc.* 142 (2001) A482-A489.
35. B. Cheng, X.L. Chen, X.W. Li, H.Y. Xu, *Int. J. Electrochem. Sci.* 7 (2012) 6453-6464.
36. H.Y. Xu, S. Xie, N. Ding, C.H. Chen, *Electrochim. Acta* 51 (2006) 4352-4357.
37. R.D. Shannon, *Acta Crystallogr. A: Cryst. Phys. Diffr. Theor. Gen. Crystallogr.* 32 (1976) p. 756.
38. F.Y. Cheng, H.B. Wang, Z.Q. Zhu, Y. Wang, T.R. Zhang, Z.L. Tao and J. Chen, *Energy Environ. Sci.* 4 (2011) 3668-3675.
39. W. Tang, X. J. Wang, Y. Y. Hou, T.V. Ree, *J. Power Sources* 198 (2012) 308-311.

40. M.D. Levi, D. Aurbach, *J. Phys. Chem. B* 101 (1997) 4630-4640.
41. K.M. Shaju, G.V. Subba Rao and B.V.R. Chowdari, *J. Mater. Chem.* 13 (2003) 106-113.
42. A.J. Bard and L.R. Faulkner, *Electrochemical Methods*, Second ed., Wiley, New York, 2001, p. 321.

© 2012 by ESG (www.electrochemsci.org)